Available online at www.sciencedirect.com
SCIENCE DIRECT
Physica C 441 (2006) 51–56
PHYSICA C
www.elsevier.com/locate/physc

Evidence for non-linear BCS resistance in SRF cavities ☆,☆☆

P. Bauer [a,*], N. Solyak [a], G.L. Ciovati [b], G. Eremeev [c], A. Gurevich [d], L. Lilje [e], B. Visentin [f]

[a] *Fermilab, Batavia, IL 60510, USA*
[b] *TJNAF, Newport News, USA*
[c] *Cornell University, Ithaca, USA*
[d] *University of Wisconsin, Madison, USA*
[e] *DESY, Hamburg, Germany*
[f] *CEA, Saclay, France*

Available online 6 May 2006

Abstract

Very powerful RF cavities are now being developed for future large-scale particle accelerators such as the International Linear Collider (ILC). The basic model for the cavity quality factor Q-slope in high gradient SRF cavities, i.e. the reduction of Q with increasing operating electric and magnetic fields, is the so-called thermal feedback model (TFBM). Most important for the agreement between the model and experimental data, however, is which different surface resistance contributions are included in the TFBM. This paper attempts to further clarify if the non-linear pair-breaking correction to the BCS resistance [A. Gurevich, in: Pushing the Limits of RF Superconductivity Workshop, ANL, September 2004; A. Gurevich, This conference.] is among those surface resistance contributions, through a comparison of TFBM calculations with experimental data from bulk Nb cavities built and tested at several different laboratories.

Keywords: Linear collider; Superconducting RF cavities; Niobium; RF surface resistance; Non-linear BCS resistance

1. The thermal feedback model

The small but finite amount of heat deposited on the inner surface of the superconducting RF cavity during operation is conducted through the cavity wall and into the liquid helium bath surrounding the cavity. In the TM01 mode the heat is mostly generated in a wide strip around the equator area, where the magnetic field (and thus the surface current) peaks. The peak field area is wide enough to allow for a one-dimensional representation of the thermal problem. The temperature profile across the Nb bulk and the temperature drop across the Nb–helium interface (with the cavities usually operating in superfluid helium the thermal impedance of the helium can be neglected) can be calculated exactly from the steady state heat balance equation and the temperature dependent thermal properties, thermal conductivity $\kappa(T)$ and Kapitza interface conductance h_{Kap}. The thermal diffusivity of high purity, polycrystalline Nb at 2 K is of the order of 0.01 m^2/s, which, for mm thick walls, gives msec thermal equilibration times. RF pulses are typically of that length (or longer) and therefore the process is reasonably well described as a steady state.

The following briefly summarizes the TFBM (a more detailed discussion can be found in [1]). We solve the following steady state heat balance equation, which contains heat conduction and generation terms:

$$\frac{\partial}{\partial x}\kappa(t)\frac{\partial T}{\partial x} + P_{\mathrm{diss}}(T_{\mathrm{m}}, H_{\mathrm{c}}, \ldots)\delta(x) = 0 \tag{1}$$

$$P_{\mathrm{diss}} = \frac{1}{2}R_{\mathrm{s}}(T_{\mathrm{m}})H_{\mathrm{RF}}^2 \tag{2}$$

☆ Supported by the US Department of Energy.
☆☆ The work at Cornell University is supported by the National Science Foundation.
* Corresponding author.
E-mail address: pbauer@fnal.gov (P. Bauer).

0921-4534/$ - see front matter © 2006 Elsevier B.V. All rights reserved.
doi:10.1016/j.physc.2006.03.056

where the delta-function in Eq. (1) reflects the fact that the RF heating is concentrated in a very thin surface layer of thickness $\lambda \cong 40$ nm, and λ is the London penetration depth. The RF power dissipated per unit area in the cavity depends on the RF magnetic field amplitude H_{RF} and the (temperature dependent) RF surface resistance $R_s(T)$ as given by Eq. (2). The equation assumes that the loss is due to the RF shielding currents only and neglects the contribution by electric surface fields (and associated dielectric loss for instance).

The solution of Eq. (1) depends on the surface temperatures on both sides of the Nb sheet of thickness d. The temperature on the RF exposed side, T_m, drives the surface resistance, while the temperature on the helium side, T_s (together with the bath temperature T_0) drives the Kapitza interface conductance. They can be derived exactly from the boundary conditions (Eqs. (3) and (4)) for a given H_{RF}, T_0 and $R_s(T_m,H_{RF},\ldots)$.

$$h_{Kap}(T_s,T_0)(T_s-t_0)d=\int_{T_s}^{T_m}\kappa(T')\mathrm{d}T' \tag{3}$$

$$\frac{1}{2}R_s(T_m,H_{RF},\ldots)H_{RF}^2=k_{Kap}(T_s,T_0)(T_s-T_0) \tag{4}$$

In this work we use exact, numerical solutions of Eqs. (3) and (4), unlike simplified TFB-models which have been often used in the literature.

The exponential temperature dependence of the BCS resistance is at the core of thermal feedback. The increase of the surface resistance with field is the result of a feedback process by which the surface temperature increases due to RF heating, while the RF heating increases with surface temperature. In this process the cavity surface temperature increases as the applied RF magnetic field increases until thermal run-away occurs. The thermal model therefore can predict the applied RF magnetic field at which the cavity quenches. The quench field due to thermal feedback is typically referred to as "thermal quench field" H_b (as opposed to the superconductor critical field, H_c). The TFBM is only as good as the surface resistance and thermal parameter models that are put in. We will discuss here the effect of the field dependence of $R_s(H_{RF})$ due to RF pair-breaking in the absence of vortex penetration [1,2] on thermal breakdown of Nb cavities.

2. RF surface resistance

The RF surface resistance of bulk, high purity Nb in the superconducting state is very small but cannot be neglected. It is usually defined as a sum of the BCS resistance $R_{s,BCS}$, and the residual resistance R_{res}. Other contributions due to field enhancement at grain edges, magnetic flux or vortices trapped at grain boundaries can also be added (a review of different surface resistance contributions can be found in [3]). The BCS RF surface resistance results from the interaction between the RF electric field (localized in a surface layer defined by the London penetration depth λ) and thermally activated electrons in a superconductor:

$$R_{s,BCS}^{lin}(T)=\frac{A\omega^2}{T}\mathrm{e}^{-\frac{\Delta}{k_bT}} \tag{5}$$

where $\Delta \cong 1.5$ meV is the superconducting energy gap, and the factor A depends on frequency (weakly) and also on Δ, λ, the coherence length ξ ($\xi \cong \lambda$ for Nb), and the mean free path l. The superconducting material parameters may vary strongly throughout λ due to the presence of metallic oxides and defects on the surface and along grain boundaries [4]. Therefore, in the absence of exact materials parameter profiles at the cavity surface, the linear BCS surface resistance is typically written in the form of Eq. (5) with the understanding that the A and Δ are actually averaged over λ.

Eq. (5) gives the linear BCS surface resistance, i.e. the BCS contribution at H_{RF} much lower than the critical field H_c. At RF fields approaching H_c the coherent motion of the Cooper pairs constituting the shielding current causes a reduction of the effective gap in the quasiparticle spectrum, greatly increasing the density of thermally activated electrons and thus the BCS loss. The non-linear BCS surface resistance for a type-II superconductor ($\lambda > \xi$) at low frequencies $\hbar\omega \ll \Delta$ in the clean limit can be obtained in the form [2]:

$$R_{s,BCS}^{nlin}(T,B)=\frac{8R_{s,BCS}^{lin}(T)}{\pi\beta^2(T)h^2}\left[\int_0^{\pi}\sinh^2\left[\frac{\beta(T)h}{2}\cos(t)\right]\tanh^2(t)\mathrm{d}t\right]$$
$$\beta(T)=\frac{\pi}{2^{3/2}}\frac{\Delta}{k_bT},\quad h=\frac{H_{RF}}{H_{c,0}} \tag{6}$$

The integral can be solved analytically for small and large βh, where $h<1$ is the reduced magnetic field:

$$R_{s,BCS}^{nlin1}(T,H_{RF})=R_{s,BCS}^{lin}(T)\left[1+\frac{\beta^2}{48}\left(\frac{H_{RF}}{H_{c,0}}\right)^2\right],\quad \beta h\ll 1 \tag{7}$$

$$R_{s,BCS}^{nlin2}(T,H_{RF})=R_{s,BCS}^{lin}(T)\left[\frac{4\mathrm{e}^{\beta\frac{H_{RF}}{H_{c,0}}}}{\beta^{7/2}\sqrt{2\pi}}\right]\left(\frac{H_{c,0}}{H_{RF}}\right)^{7/2},\quad \beta h\gg 1 \tag{8}$$

For low fields, $\beta h \ll 1$, the first non-linear correction is quadratic in H_{RF}, while for high fields $\beta h \gg 1$, the non-linear BCS resistance increases exponentially. The BCS resistance, which is strongly temperature dependent, can be derived from Q measurements in the cavity at different temperatures. The fit of the temperature dependence of the surface resistance allows separation of the temperature dependent (BCS) and independent (residual) surface resistance contributions. This procedure is easiest (and usually applied) at low field where it yields A and Δ in R_{BCS}^{lin}. At high fields the non-linearity of R_s makes the procedure more involved and ambiguous.

The non-linear BCS surface resistance is defined by Eqs. (6)–(8) for the clean-limit ($l \gg \xi_0$) only. Taking into account impurity scattering is a much more complicated problem, but a first order quadratic correction to the

non-linear BCS resistance for arbitrary mean free path can be obtained in the form similar to Eq. (7):

$$R^{\mathrm{nlin1}}_{\mathrm{s,BCS}}(T,B) = R^{\mathrm{lin}}_{\mathrm{s,BCS}}(T)\left[1 + C(l,\omega,T)\left(\frac{H_{\mathrm{RF}}}{H_{\mathrm{c}}}\right)^2 + \cdots\right], \tag{9}$$

where $C(l,\omega,T)$ is now a function of the mean free path, and $H_{\mathrm{c}}(T)$ is the thermodynamic critical field at the operating temperature. In the clean limit C is of the order of unity in Nb at $T \cong 2\,\mathrm{K}$ and increases as the temperature decreases (see Eq. (7)). Note that the larger C becomes, the smaller the field range in which the first order expansion in Eq. (9) is valid. Generally, C decreases as l decreases, that is, the BCS non-linearity becomes less pronounced as the surface layer gets more contaminated with impurities. Given our lack of information about the mean free path at the cavity surface, Eq. (9) can be used in TBM calculations in which C is regarded as a fit parameter.

3. Thermal parameters

Fig. 1 shows different model implementations of the thermal conductivity of polycrystalline, high purity Nb, consistent with experimental data. Instead of using a full-blown model (such as presented by Koechlin and Bonin [6]) we used the following simple fit, which also takes into account a "mild" phonon peak:

$$\kappa(T) = 0.7\mathrm{e}^{1.65T-0.1T^2}\left(\frac{\mathrm{W}}{\mathrm{K}\cdot\mathrm{m}}\right) \tag{10}$$

Similarly we used a phenomenological fit for the Kapitza interface conductance, such as proposed by Mittag [7], for $T - T_0 < 1.4\,\mathrm{K}$:

$$h_{\mathrm{Kap}}(T,T_0) = 200\cdot T^{4.65}\left[\begin{array}{l} 1 + 1.5\left(\frac{T-T_0}{T_0}\right) + \cdots \\ \cdots + \left(\frac{T-T_0}{T_0}\right)^2 + 0.25\left(\frac{T-T_0}{T_0}\right)^3 \end{array}\right] \times \left(\frac{\mathrm{W}}{\mathrm{K}\cdot\mathrm{m}^2}\right) \tag{11}$$

We also simulated some 4.2 K cases, where we used $h_{\mathrm{He}} = 20T^3\ \mathrm{W/m^2/K}$ instead of Eq. (11), consistent with literature data for strong free convective heat transfer in pool boiling helium I [8].

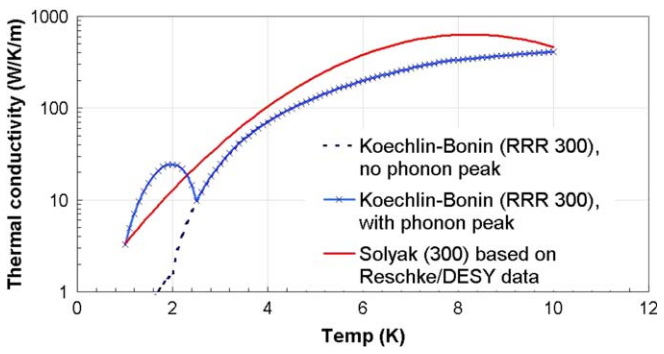

Fig. 1. Thermal conductivity of high purity Nb (RRR = 300) according to Koechlin–Bonin and the simpler fit ("Solyak-fit", Eq. (10)) used in the calculations presented here.

4. Model versus cavity data

The following presents a comparison of the model with experimental data. The model involves the exact numerical solution of Eqs. (3) and (4) with the full non-linear dependence $R_{\mathrm{s}}(H_{\mathrm{RF}})$ given by Eq. (6). We used the linear BCS surface resistances measured in the cavities at low field to obtain the input parameters A and Δ both in the clean limit (Eq. (6)) and the low-field dirty limit approximation given by (Eq. (9)). In the absence of exact knowledge of the mean free path in the contaminated surface layer, the C parameter in Eq. (9) was varied to fit the data in the medium field region (~60–120 mT). The linear BCS fit parameters A and Δ as well as $R_{\mathrm{s,res}}$ and the clean-limit, non-linear BCS parameter β are listed together with the thermal conductivity and Kapitza conductance in Table 1. The thermal parameters were calculated at the bath temperature for illustration purposes. The parameters for the linear BCS (Eq. (5)) and the residual resistance were derived from fits of measurements of the surface resistance as function of temperature at low field for each cavity respectively. Note that the ratios $\Delta/k_{\mathrm{b}}T_{\mathrm{c}}$ found from this procedure are usually ≅2, about 10–15% higher than the BCS value of 1.764, which indicates the significance of strong electron–phonon coupling effects in Nb. Note that this value presumably includes some gap energy reduction due to the presence of metallic oxides and interstitial impurities. The residual resistance is the value to which the low field $R_{\mathrm{s}}(T)$ approaches at very low temperature, where the BCS resistance vanishes. The β parameter was calculated with the respective Δ obtained from the low field fits of the linear BCS resistance. The material parameters ξ_0, λ_0 were assumed to be 40 nm. The values of the parameter C in Eq. (9) were derived from a data fit in the mid-field region. In some cases the Q-slope in the medium field region even exceeded the Q-slope prediction on the basis of the non-linear BCS model in the clean limit (worst case). In this case no such fits were performed (and C parameters are omitted in the table). Calculations with $C, \beta \neq 0$ were performed for RF fields $H_{\mathrm{RF}} < 160\,\mathrm{mT}$ to remain well below the critical field. Note that all models used here assume uniform surface properties.

The most important criteria the experimental data needed to satisfy for this comparison is that they had to be state of the art and have as little low and medium field Q-slope as possible, such as to minimize the extrinsic effects and limit the surface resistance to the basic residual and BCS components. The latter condition would obviously improve the model/data agreement, with the model using only BCS (and residual) resistance. All the cavity experimental results discussed here were chosen with these criteria in mind. For some cavities we had data both at ~2 K and ~4.2 K. Most cavities were single-cell prototypes, with the only exception being the DESY AC70, which is a full-length 9-cell TESLA

Table 1
TFBM parameters for cavity Q calculation

Process	C-103 CEA EP	C-115 CEA EP	D-AC70 DESY EP	F-3C-1 FNAL BCP	J-LLSC JLAB BCP	J-OCSC JLAB BCP	CU-LE1-30 CORNELL BCP
T_0 (K)	1.44	1.6	2 (1.9)	1.8	2.0	1.4	1.53 (1.75)
G (Ω)	283	283	270	291	282	273	255
d (mm)	2.6	2.6	2.6	2.6	2.6	2.6	2.75
$\kappa(T_0)$ (W/K/m)	6.1	7.6	11.22	9.9	12.7	5.8	6.9 (9.3)
$h_{\mathrm{Kap}}(T_0)$ (W/K/m^2)	1090	1780	3956	3080	5021	956	1445 (2699)
R_{res} (nΩ)	3.2 (4.2)	1 (2)	−10 (5.2)	10	17 (9.4)	5 (3.6)	11 (11)
$R_{\mathrm{bcs,lin}}(T_0)$ (nΩ)	0.5 (0.3)	1.7 (1.05)	24 (4.3)	40	31 (20)	3.9 (5.1)	5.6 (1)
$\Delta/k_{\mathrm{b}}T_{\mathrm{c}}$	2 (2.05)	1.97 (1.93)	1.53 (1.94)	1.92	2.1 (1.94)	2.09 (2.15)	1.99 (1.99)
A (10^{-6} ΩK/(GHz^2))	3.28 (2.53)	2.97 (1.42)	0.71 (1.25)	1.95	3.93 (1.52)	3.98 (2.13)	3.30 (2.23)
T_{c} (K)[a]	9.2	9.2	9.2	9.2	9.2	9.2	9.2
$\omega/2\pi$ (GHz)	1.3	1.3	1.3	3.9	1.5	1.5	1.5
β	14.2 (14.5)	12.6 (12.3)	7.8 (10.4)	11	10.7 (9.9)	15.3 (15.7)	13.3 (11.6)
C ($\mu_0 H_{\mathrm{c}} = 180$ mT)[a]	–	3.6 (3.4)	1.5 (2.5)	0	2.6 (2.2)	–	–
$\mu_0 H_{\mathrm{c},0}$ (mT)[a]	200	200	200	200	200	200	200

Linear ($\Delta/k_{\mathrm{b}}T_{\mathrm{c}}$, A, Eq. (5)) and non-linear BCS resistance (β, Eq. (6) and C, Eq. (9)), thermal conductivity (κ, Eq. (10)) and Kapitza conductance (h_{Kap}, Eq. (11)). Data out (inside) parentheses are for before (after) the low temperature bake.
[a] Assumed values [5].

cavity. The Saclay and DESY cavities were electro-polished, while the J-Lab, Cornell and FNAL cavities were BCP etched. The J-Lab cavities and the Saclay cavity C115 were also post-purified (heat treated at ~1400 °C in the presence of Ti to increase RRR). The thermal conductivity $\kappa(T)$ was not modified to account for the increased RRR. This would have further complicated the model without changing much in the results from the calculation (the thermal parameters affect strongly the thermal quench field, and only marginally the medium field Q-slope)[1]. The data obtained before and after the low temperature bake (~120 °C, 50 h) are presented. Essentially all Q measurements were performed in the CW (=steady state) mode.

The Q versus peak magnetic field (at the equator) data and calculation results are shown in Figs. 2–8. The cases of before and after baking are shown in separate plots. Typically three sets of model calculations are plotted: (1) using the linear model (Eq. (5)) in blue, (2) using the quadratic approximation of the model for general mean free path (Eq. (9)) in red and (3) using the non-linear model in the clean limit (Eq. (6)) in orange. In the 4.2 K cases only models (1) and (3) are shown.

5. Discussion

The different data-model comparisons need to be evaluated on a case-by-case basis. However, certain trends can be identified:

[1] An issue, which was reported in the context of the CU cavity LE1-30 (Fig. 3), is due to a possible increase of the bath temperature during the testing (50 mK in LE1-30). We calculated that a bath temperature increase by 500 mK with $T \sim T_0(1 + h^2)$, would be required at the reduced field $h = 1$ to explain the Q-drop in the after baking condition even after including the quadratic non-linear BCS (Eq. (9), $C \sim 3$) and residual resistance. Since this is much more than the observed bath temperature change, this effect was not considered any further in the calculations.

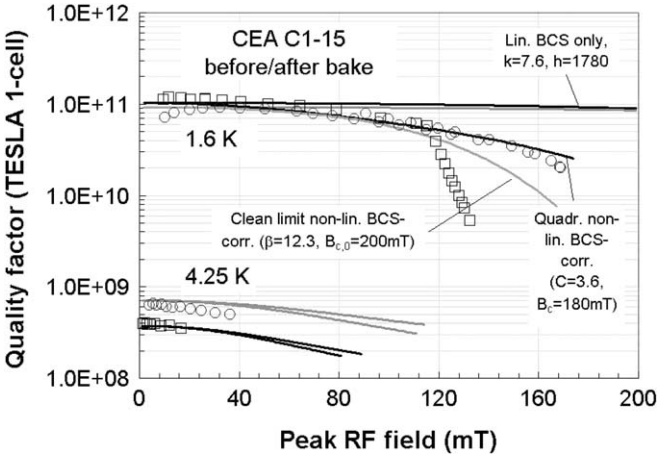

Fig. 2. Comparison of measured and predicted quality factor of a CEA/Saclay single cell TESLA cavity (C-115) before (top) and after (bottom) baking. Experimental data were obtained at 1.6 K and 4.25 K. The cavity was electro-polished and post-purified and has a very small residual surface resistance.

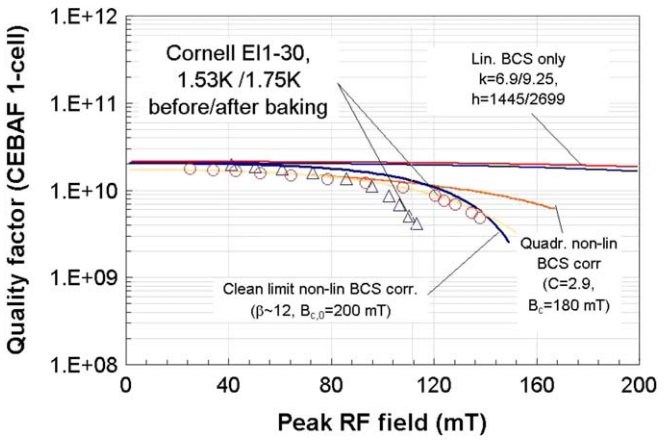

Fig. 3. Comparison of measured and predicted quality factor of a Cornell University single cell CEBAF cavity (LE1-30) before (top) and after (bottom) baking. Experimental data were obtained at 1.53 K before and 1.75 K after baking. The bath temperature increased by ≅50 mK during the test.

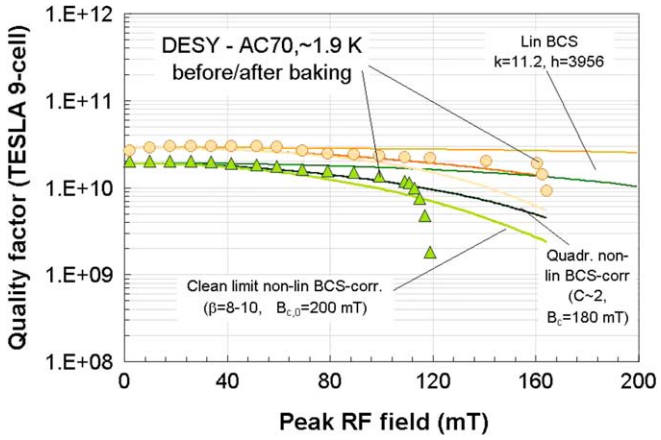

Fig. 4. Comparison of measured and predicted quality factor of a DESY 9-cell TESLA cavity (AC70) before (top) and after (bottom) baking. Experimental data were obtained at ~1.9 K. The cavity was electro-polished.

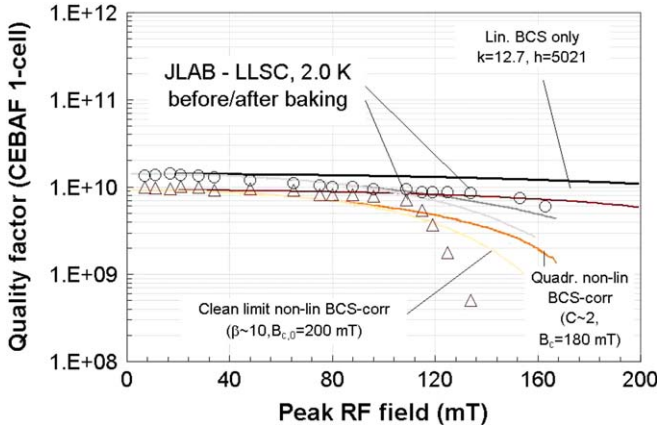

Fig. 5. Comparison of measured and predicted quality factor of a JLAB low loss, single cell CEBAF cavity (LLSC, 1.5 GHz) before (top) and after (bottom) baking. Experimental data were obtained at 2.0 K.

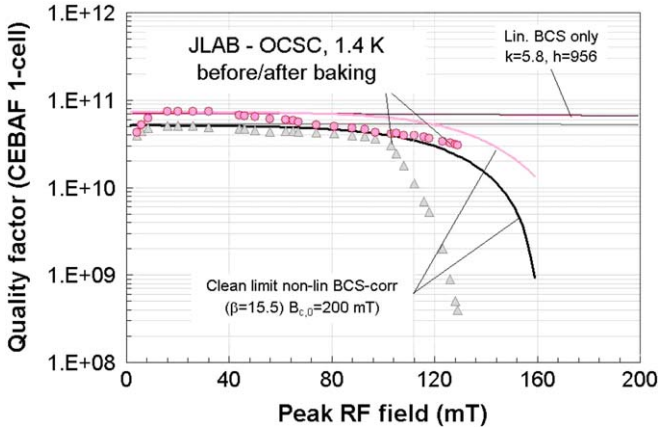

Fig. 6. Comparison of measured and predicted quality factor of a JLAB single cell CEBAF cavity (OCSC – original CEBAF shape, 1.5 GHz) before (top) and after (bottom) baking. Experimental data were obtained at the very low temperature of 1.4 K, which explains the high Q.

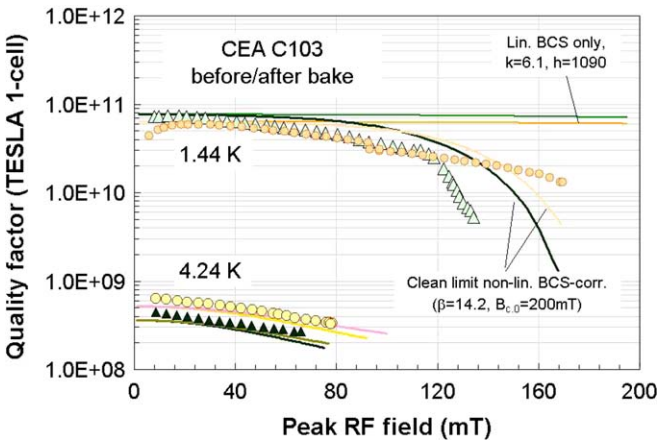

Fig. 7. Comparison of measured and predicted quality factor of a CEA/Saclay one-cell TESLA cavity (C 103) before (top) and after (bottom) baking. Experimental data were obtained at 1.44 K and 4.2 K temperature.

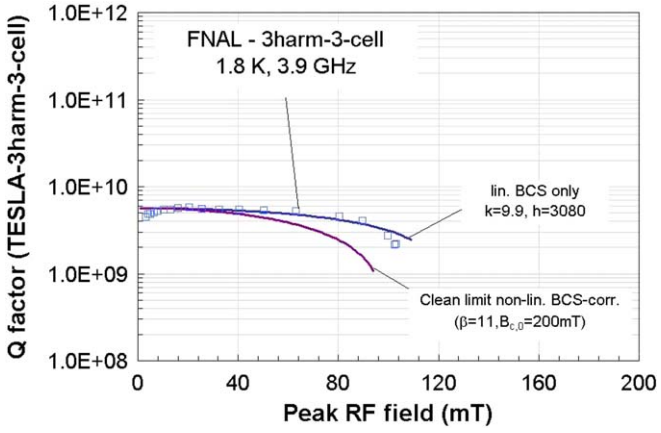

Fig. 8. Comparison of measured quality factor of a Fermilab 3rd harmonic (3.9 GHz) 3-cell cavity to model predictions. Experimental data were obtained at 1.8 K. There are no after baking data.

- The clean limit non-linear resistance model, which produces the strongest Q-slope at high field, predicts the Q best in the lowest temperature cases shown in Figs. 3, 6 and 7.
- For ~2 K cases, the medium field Q is better described by Eq. (9) with $C \cong 1-4$ in the medium field region (Figs. 2, 4 and 5). The non-linear, clean limit model usually predicts a too strong Q-slope.
- As reported before (e.g., in [9]) TFB models based on the linear BCS resistance strongly under-estimate the medium-field Q-slope and over-estimate the quench field[2]. The only exception is the Fermilab 3rd harmonic case (Fig. 8) where the data before baking are consistent with linear BCS resistance only. Moreover, TFBM

[2] TFBM quench field predictions on the basis of linear BCS only are by a factor ~2 larger than the fields to which the measurements are limited.

based on linear BCS resistance correctly predicts the thermal quench field as well. Note, however, that the 3rd harmonic cavity operates at the "unusually" high frequency of 3.9 GHz.

- The good agreement between the model and data at 4.2 K in Figs. 2 and 7 indicates that in these cases the surface resistance is BCS dominated. Indeed, no evidence of abrupt kinks on the $Q(H_{RF})$ curves is consistent with the lack of vortex penetration in the field range where $Q(H_{RF})$ was measured. At 4.2 K the non-linear BCS contribution is suppressed, which is also consistent with Eq. (6).
- All before baking $Q(H_{RF})$ curves in Figs. 2–7 exhibit a kink around 80–120 mT, followed by a precipitous reduction in Q (the so-called Q-drop), which cannot be described by the BCS model discussed here[3]. This abrupt decrease in $Q(H)$ indicates an additional mechanism of RF dissipation, which turns on at higher fields. We suggest that this extra dissipation most likely results from vortex penetration above $H_{RF} \sim 100$ mT at grain boundaries, surface grooves or steps, or isolated regions on the cavity surface where the thickness of pentooxide layer or impurity (O, H, etc.) concentration is increased. As a result, vortices are mostly driven by RF field in and out of those localized hotspots on the cavity surface, which have been revealed by temperature maps of Nb cavities. In turn, such hotspots ignited above the onset of vortex penetration $H_{RF} \sim 100$ mT can significantly increase the high-field Q-slope [2].
- The fact that the kinks on the $Q(H)$ curves disappear after baking indicates that baking may remove or ameliorate a significant fraction of the hotspots present in before-baked cavities. There are many possible mechanisms by which hotspots could be eliminated by baking, for example, diffusion of quenched Cottrell atmospheres of impurities away from grain boundaries, diffusion of oxygen from the surface into the bulk, etc.
- Aside from the kinks in the $Q(H)$ curves, which are likely due to inhomogeneous thermal breakdown initiated by vortex penetration in hotspots, the TFB model with the field dependent Rs(HRF) provides a reasonably good description of our observation. For example, low and medium field portions of the $Q(H_{RF})$ curves are described well even for cavities before baking. The agreement between the model and experiment significantly improves for baked cavities, consistent with our interpretation given above.

6. Conclusions

Calculations based on the TFBM were implemented and applied to the case of the state of the art SRF cavities from CEA, DESY, J-Lab, CU and FNAL. This comparison reveals that incorporation of the non-linear BCS resistance into the TFBM significantly improves the agreement with observed $Q(H_{RF})$ curves at medium fields, and sometimes at high fields as well.

The TFB calculations with the uniform BCS resistance cannot predict the ultimate Q-drop before baking. This indicates that other mechanisms like vortex penetration in hot spots could turn on at higher fields. Yet, the medium field Q-slope before baking and the medium and high field Q-slope after baking in tested cavities are reasonably well described by the uniform non-linear BCS resistance. Our data suggest that the agreement between the model and experiment can be further improved if impurity scattering in the contaminated surface layer is taken into account.

References

[1] A. Gurevich, in: Pushing the Limits of RF Superconductivity Workshop, ANL, September 2004.
[2] A. Gurevich, Physica C, this conference, doi:10.1016/j.physc.2006.03.024.
[3] P. Bauer et al., FNAL Tech Div Memo TD-04-014, 12/04. Available from: <http://www-td.fnal.gov/info/td_library.html>.
[4] J. Halbritter, 11th RFSCWS, Luebeck, 2003.
[5] S. Casalbuoni et al., Nuclear Instruments and Methods in Physics Research A 538 (2005) 45–64.
[6] F. Koechlin, B. Bonin, CEA internal note DAPNIA-SEA-96-01, January 1996.
[7] H. Mittag, Cryogenics 13 (1973) 94.
[8] S. Van Sciver, Helium Cryogenics, Plenum Press.
[9] B. Visentin, in: 11th RFSCWS, Luebeck, 2003 or G. Ciovati, in: Pushing the Limits Workshop, ANL, September 04.

[3] If the observed non-isothermal low-field R_s is expressed phenomenologically in the form $R_s(H) = R_{BCS}[1 + \gamma(H_{RF}/H_c)^2]$, the TFBM on the basis of the linear BCS predicts $\gamma \cong 0.25$, while the data after baking are better described by $\gamma \cong 1 - 4$. In the before baking cases this applies only to the medium field slope, while a very strong Q-drop at high fields would require $\gamma \cong 500$. The variation of thermal properties in TFMB by factors ~2 cannot account for the difference in γ.